Article

pubs.acs.org/Biomac

Conformational Preferences of the O-Antigen Polysaccharides of *Escherichia coli* O5ac and O5ab Using NMR Spectroscopy and Molecular Modeling

Anita Sarkar,[†,‡] Carolina Fontana,[‡,§] Anne Imberty,[†] Serge Pérez,*[,†] and Göran Widmalm*[,§]

[†]Centre de Recherches sur les Macromolécules Végétales - CNRS, affiliated with Université Grenoble and ICMG, BP 53 X, 38041 Grenoble Cedex, France

[§]Department of Organic Chemistry, Arrhenius Laboratory, Stockholm University, S-106 91, Stockholm, Sweden

Supporting Information

ABSTRACT: *Escherichia coli* serogroup O5 comprises two different subgroups (O5ab and O5ac), which are indiscernible from the point of view of standard immunological serotyping. The structural similarities between the O-antigen polysaccharides (PSs) of these two strains are remarkable, with the only difference being the glycosidic linkage connecting the biological tetrasaccharide repeating units. In the present study, a combination of NMR spectroscopy and molecular modeling methods were used to elucidate the conformational preferences of these two PSs. The NMR study was based on the analysis of intra- and inter-residue proton−proton distances using NOE build-up curves. Molecular models of the repeating units and their extension to polysaccharides were obtained, taking into account the conformational flexibility as assessed by the force field applied and a genetic algorithm. The agreements between experimentally measured and calculated distances could only be obtained by considering an averaging of several low energy conformations observed in the molecular models.

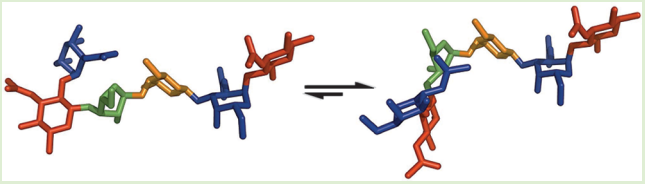

INTRODUCTION

Escherichia coli are Gram-negative bacteria part of the normal human intestinal microflora. They are usually nonpathogenic, but some strains have acquired virulence factors that allow them to cause diarrheal diseases, urinary tract infections, and sepsis/meningitis.[1] The polysaccharides on the surface of microbial pathogens are one of the major targets of the host's immune response upon infection, and the generation of specific antibodies directed against these antigens confers protection against the disease. In Gram-negative bacteria, the serological specificity provided by the O-antigen polysaccharide moiety of the lipopolysaccharides (LPSs) is used to classify different serogroups. The serotyping is based on the reactivity of an unknown O-antigen with polyclonal antisera elicited in rabbits by the O-antigens of different reference strains of *E. coli*.[2−4] The antiserum usually consists of a heterogeneous population of antibodies that recognize and bind to different epitopes of the same antigen and can be classified in two groups: (a) antibodies that bind to internal epitopes and (b) antibodies that bind to terminal epitopes.[5,6] The specificity of these antibodies will also determine the cross-reactivity capacity between different O-antigen polysaccharides displaying similar epitopes. Thus, not only the structure but also the conformational behaviors of the O-antigen polysaccharides (PSs) are of key importance to understand the role of these glycans in serological cross-reactivity.

Cross-reactivities have been observed quite often between different *E. coli* serogroups,[4] and attributed to structural similarities in the O-antigen polysaccharides. According to standard immunological serotyping, the *E. coli* strain 180/C3 was classified as belonging to the serogroup O5,[7] however, the structural elucidation of its O-antigen PS revealed a very similar but not identical structure to that reported previously by MacLean and Perry.[8] The structural difference between these two strains was used as an argument to divide the serogroup O5 in the two different subtypes named O5ac and O5ab. In addition to the strong cross-reactivity observed between these two subgroups, it has also been reported that the O5 serogroup shows cross-reactivity with the O7, O65, O70, O71, and O114 serogroups.[4]

The O-antigen polysaccharides of *E. coli* O5ac and O5ab are composed of linear tetrasaccharide repeating units, which are very similar to each other (Figure 1):[7,8]

→2)-*β*-D-Qui*p*3NAc-(1→3)-*β*-D-Rib*f*-(1→4)-*β*-D-Gal*p*-(1→3)-*β*-D-Gal*p*NAc-(1→ (O5ac)[8]

→4)-*β*-D-Qui*p*3NAc-(1→3)-*β*-D-Rib*f*-(1→4)-*β*-D-Gal*p*-(1→3)-*β*-D-Gal*p*NAc-(1→ (O5ab)[7]

The only difference between these two polysaccharides is the substitution pattern of the *β*-D-Qui*p*3NAc residue, which is 2-substituted in O5ac and 4-substituted in O5ab. Considering that the biosynthesis most probably takes place by the Wzx/Wxy-dependent pathway, the GalNAc residue is expected to be

Received: March 8, 2013
Revised: May 21, 2013
Published: May 30, 2013

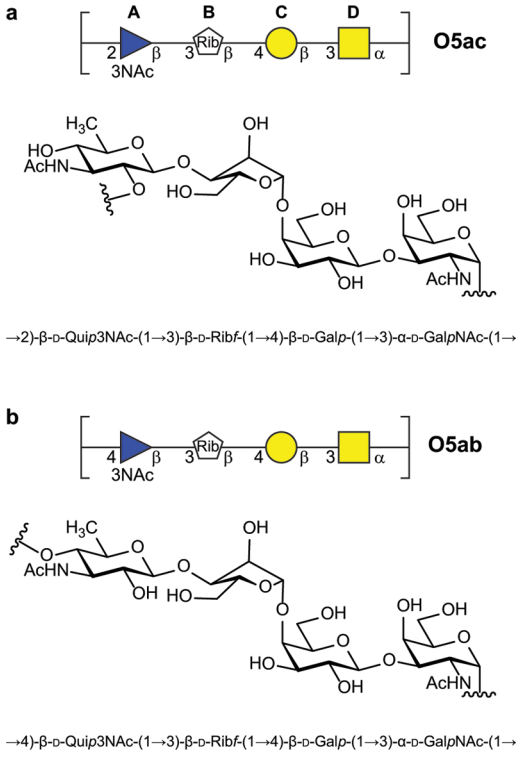

Figure 1. Structures of the biological repeating units of the O-antigen PSs of **a**) *E. coli* O5ac and **b**) *E. coli* O5ab. Each structure is represented in CFG notation (*top*), schematic chemical representation (*middle*) and standard nomenclature (*bottom*).

located at the reducing end of the biological repeating unit.[9] Thus, these two polysaccharides are positional isomers that differ only in the glycosidic linkage connecting biological repeating units, and as a consequence, they will display identical terminal epitopes on the cell surface. As shape and biological function of polysaccharides are closely related, an understanding of the conformational behaviors of the bacterial surface polysaccharides in solution can clearly help to elucidate this relationship. Herein, we focus our study on the O-antigen cell surface polysaccharides of *E. coli* O5ac and O5ab in an attempt to understand their serological similarities.

EXPERIMENTAL SECTION

Definitions. The torsion angles describing the glycosidic linkages were defined as follows: Φ_{O5} = O5−C1−O1−C*x*, Φ_H = H1−C1−O1−C*x*, $\Psi_{C(x+1)}$ = C1−O1−C*x*−C(*x* + 1), and Ψ_H = C1−O1−C*x*−H*x*, where *x* is the linkage position of the adjacent sugar residue. The different conformational families were denoted Ψ_H^+, Ψ_H^-, Ψ_H^{cis}, and Ψ_H^{trans} according to the state of their characteristic Ψ_H torsion angles (*gauche* +, *gauche*−, *cis*, and *trans*, respectively). Analogously, the conformational families that have a torsion angle Φ_H in the *trans* state were denoted Φ_H^{trans}.

Starting Models. The Gal*p* and Gal*p*NAc monosaccharides were obtained from the Glyco3D database (http://glyco3d.cermav.cnrs.fr/). The two conformers ($^3T_4$ and $^OT_1$) of *β*-D-Rib*f* were extracted from files found in the RCSB Protein Data Bank[10] (PDB ID: 3KSM and 1QXB, respectively). The *β*-D-Qui*p*3NAc monosaccharide was built from the *α*-D-Qui*p* structure extracted from a PDB file (PDB ID: 1MMY) and *N*-acetylated using an optimized NAc fragment from Glyco3D. Oligosaccharide models, representing the repeating units of the O-antigen PSs of *E. coli* O5ac and O5ab, were built taking in consideration the tetrasaccharide biological repeating unit (see Figure 1) and two additional monosaccharide residues (one at the reducing and the other at the terminal end) required to represent the glycosidic linkage between two biological repeating units. For each O-antigen PS, two starting models were constructed, each with a different conformation of the Rib*f* residue. The torsion angles describing the four glycosidic linkages were initially set to values found in structures of similar characteristics[11] or obtained from models found in Glyco3D database. All disaccharides and oligosaccharides models were built using the software SYBYL X 1.3 (Tripos Inc., St. Louis, MO).

Energy Calculations. The geometry optimizations of the starting mono-, di-, and oligosaccharides were performed using the Tripos force field,[12] with the PIM partial atomic charges[13] and an energy convergence criterion of 0.05 kcal/mol·Å for a maximum of 1000 iterations for monosaccharides and 10000 iterations for oligosaccharides. The dielectric constant was set to 4.0.

Conformational Analysis of Oligosaccharides. The conformational space available to the hexasaccharide models was characterized using the software SHAPE.[14] Within SHAPE, MM3[15,16] and the block diagonal minimization method for geometry optimization were used with the default energy convergence criterion ($\Delta E = 0.00008 \times n$ kcal/mol·Å every five iterations, where *n* = number of atoms). MM3 allows full relaxation of the glycosidic residues taking into account the *exo*-anomeric effect,[16,17] and this force field also allows optimization to a nearby transition state (with the full matrix Newton−Raphson method).

Genetic Algorithm. The systematic exploration of the conformational search of the hexasaccharide models was performed using the software SHAPE. The genetic algorithm parameters for conformer generation were specified to a population size of 25 individuals to be included in every population throughout the search, while the total number of parallel populations to be used during the search was set to 20. Every generation produced by the genetic algorithm was comprised of the total number of individuals = population size × total number of populations.

The energy convergence criterion for the conformers generated was assigned a window size of 20 to search for improvements (i.e., the search was terminated when even after 20 generations no significant improvements in conformational energy was found), with a limit value of −0.5 kcal/mol, that is, the highest energy difference in the entire window that is accepted as a significant improvement for the search to continue.

Preparation and Purification of the O-Antigen PSs. The O-antigen PSs from *E. coli* O5ac and O5ab were available from a previous study.[7] Purification by size exclusion chromatography was carried out on a HiLoad 16/60 Superdex 30 column (GE healthcare) using an ÄKTA purifier system (GE healthcare).

NMR Spectroscopy. The O-antigen PS from *E. coli* O5ac (3.6 mg) was deuterium-exchanged by repeated cycles of dissolution of the sample in excess of 99.9% D_2O followed by freeze-drying. The sample was dissolved in 0.5 mL 99.9% D_2O and treated with a Chelex 100 cation exchange resin (100−200 mesh, Na^+ form, BioRad) for 1 h in order to remove paramagnetic ions. The solution was filtered to a 5 mm NMR tube, freeze-dried, and redissolved in 0.6 mL of 99.99% D_2O; sodium 3-trimethylsilyl-(2,2,3,3-$^2H_4$)-propanoate (TSP) was added as internal reference (δ_H 0.00). Oxygen was removed by three freeze−pump−thaw cycles, and finally, the NMR tube was flame-sealed under vacuum. ^{1}H NMR chemical shifts assignments of the PS were reported previously.[7]

Proton−proton cross-relaxation rates were measured using a 2D ^{1}H,^{1}H-NOESY experiment with a zero-quantum suppression filter[18] on two different spectrometers: a Bruker Avance III 700 MHz and a Bruker Avance 500 MHz, both equipped with 5 mm TCI (^{1}H/^{13}C/^{15}N) Z-Gradient (53.0 G·cm^{-1}) CryoProbes. The experiments were recorded at 42 °C over a spectral width of 5.0 ppm, with 14k × 256 or 10k × 260 data points (at a ^{1}H frequency of 700 and 500 MHz, respectively) using 6−16 scans per t_1 increment and a total recycle time between scans of 16 or 13 s (at a ^{1}H frequency of 700 and 500 MHz, respectively) corresponding to five times the longest T_1. Five different cross-relaxation delays (mixing times) of 30, 40, 50, 60, and 80 ms were used. For the experiments recorded at a ^{1}H frequency of 700 MHz, a 40 kHz broad and 20 ms long adiabatic[19,20] smoothed CHIRP[21] pulse was employed during the zero-quantum suppression,

accompanied by a gradient pulse of strength 9% of the maximum; for the experiments recorded at a ^{1}H frequency of 500 MHz, a 27 kHz broad adiabatic smoothed CHIRP pulse was used instead, and the gradient pulse strength was set to 6% of the maximum. Prior to Fourier transformation, forward linear prediction to 512 or 520 points (at a ^{1}H frequency of 700 and 500 MHz, respectively) in the F_1-dimension and zero-filling to 16k × 2k points were performed; 90° shifted squared sine-bell window functions were used in both dimensions. A fifth-order polynomial baseline correction was applied in both dimensions and the peaks of interest were integrated using the same integration limits at all mixing times.

The volume integral of each NOE buildup peak was divided by the volume integral of the respective autopeak to produce the normalized buildup intensities that were used to calculate the NOE buildup rates (σ) from the slope. At each magnetic field, the cross relaxation rates were averaged for each proton pair, and the unknown proton−proton distances (r_{ij}) calculated using as reference the intraresidue distance between H1 and H2 of the α-D-GalpNAc residue (**D**) and the following equation:

$$r_{ij} = r_{\mathrm{ref}} \times \left(\frac{\sigma_{\mathrm{ref}}}{\sigma_{ij}}\right)^{1/6}$$

Effective proton−proton distances from the models were calculated using the following equation:[22]

$$\frac{1}{r_{\mathrm{calc}}} = \langle r^{-6}\rangle^{1/6}$$

The final proton−proton distances were obtained by averaging the distances calculated at each magnetic field. The plots that were used to obtain the cross relaxation rates had a residual standard deviation of less than 16%. The experimental error in σ is estimated to be less than ±26%, which corresponds to only ±4% in the calculated proton−proton distances, as a result of the r_{ij}^{-6} dependence, thus being on the order of ±0.1 Å.

The O-antigen PS from *E. coli* O5ab (6.4 mg) was deuterium-exchanged by repeated cycles of dissolution of the sample in excess of 99.9% D_2O followed by freeze-drying. The sample was then transferred to a 5 mm NMR tube, freeze-dried, and redissolved in 0.6 mL of 99.99% D_2O, using sodium 3-trimethylsilyl-(2,2,3,3-$^2H_4$)-propanoate (TSP) as internal reference (δ_H 0.00). ^{1}H NMR chemical shifts assignments were reported earlier.[8]

Proton−proton cross-relaxation rates were measured at a ^{1}H frequency of 700 MHz using a selective 1D single-pulse-field-gradient spin−echo (SPFGSE) ^{1}H,^{1}H-NOESY experiment with a nulling 180° pulse[23] and a zero-quantum suppression filter.[18] The experiments were recorded at 27 °C over a spectral width of 7.5 ppm, with 21k data points and 256 scans per transient. A total recycle time between scans of 23 s corresponding to 8.3 times the longest T_1 was employed. Eight different mixing times of 45, 50, 55, 60, 65, 70, 75, and 80 ms were used. Selective excitation of the H1 proton of the α-D-GalpNAc residue (**D**) was achieved using a 40 Hz broad r-SNOB[24] shaped pulse of 80 ms, flanked by sinusoidal pulse field gradients of 1 ms length, with the strength set to 15% of the maximum. The strength of the 1 ms length gradients flanking the 180° nulling pulse during the mixing time was set to 40% of the maximum. A 40 kHz broad and 20 ms long adiabatic smoothed CHIRP pulse was employed during the zero-quantum suppression, accompanied by a gradient pulse of strength 8% of the maximum. Zero-filling to 128k points and an exponential line broadening of 1 Hz were performed prior to Fourier transformation. A fifth-order polynomial baseline correction was applied, and the peaks of interest were integrated using the same integration limits at all mixing times.

In addition, a 2D ^{1}H,^{1}H-NOESY experiment with a zero-quantum suppression filter[18] and a mixing time of 80 ms was recoded over a spectral width of 7.5 ppm, with 22k × 256 data points, using six scans per t_1 increment and a total recycle time between scans of 14 s (corresponding to 5 times the longest T_1). A 40 kHz broad and 20 ms long adiabatic smoothed CHIRP pulse was employed during the zero-quantum suppression, accompanied by a gradient pulse of strength 8% of the maximum.

The integrals of each NOE buildup peak were divided by the integral of the selectively excited peak to produce the normalized buildup intensities that were used to calculate the NOE buildup rates (σ) from the slope. The intraresidue distance between H1 and H2 of the α-D-GalpNAc residue (**D**) was used as reference for distance calibration. The plots that were used to obtain the cross-relaxation rates had a residual standard deviation of less than 2%. Although the subsequent conformational averaging for comparison to experimental NOE data utilized a limited number of conformations, this approximation still yielded very good agreements between employed models and experimental data.

The average number of repeating units of each O-antigen PS was estimated by integration of the ^{1}H NMR spectra, using resonances of the terminal β-D-Quip3NAc residue (**A′**) as a reference. Diffusion-filtered ^{1}H NMR experiments were employed to remove smaller signals originating from impurities of lower molecular mass than the O-antigen PSs. The spectra were recorded at 26 °C on a Bruker Avance III 600 MHz spectrometer equipped with a 5 mm Z-gradient (55.7 G·cm^{-1}) TXI (^{1}H/^{13}C/^{31}P) probe, using the 1D stimulated spin−echo sequence with bipolar gradients and longitudinal eddy current delay (ledbpgp2s1d).[25] The experiments were recorded with 24k data points over a spectral width of 10 ppm, using 256 and 96 scans (O-antigen PS of *E. coli* O5ac and O5ab, respectively), and a total recycle delay between scans of 15 s. The diffusion time (Δ) was set to 50 ms. Diffusion encoded sinusoidal gradient pulses (δ/2) of 1.8 ms and a strength of 60% of the maximum and an eddy current delay (T_e) of 5 ms were used. The spin system of the terminal β-D-Quip3NAc residue (**A′**) present in both PS was characterized using ^{1}H,^{1}H-TOCSY experiments with different mixing times and the resonances from H1 to H6 were found at δ_H 4.60, 3.37, 3.85, 3.19, 3.58, and 1.32, respectively.

RESULTS AND DISCUSSION

The repeating units of the O-antigen PSs of *E. coli* O5ac and O5ab comprise the same constituent monosaccharides and glycosidic linkages, with the exception being the glycosidic linkage connecting two biological repeating units (α-D-GalpNAc-(1→2)-β-D-Quip3NAc in the former and α-D-GalpNAc-(1→4)-β-D-Quip3NAc in the latter). To build the 3D hexasaccharide models, α-D-GalpNAc and β-D-Quip3NAc residues were added to the terminal nonreducing and reducing ends of the tetrasaccharide biological repeating units, respectively. Five glycosidic linkages had to be defined, three of them present in both PSs (β-D-Quip3NAc-(1→3)-β-D-Ribf, β-D-Ribf-(1→4)-β-D-Galp, and β-D-Galp-(1→3)-α-D-GalpNAc), one of them present exclusively in the O-antigen PS of *E. coli* O5ac (α-D-GalpNAc-(1→2)-β-D-Quip3NAc) and the other one in the O-antigen PS of *E. coli* O5ab (α-D-GalpNAc-(1→4)-β-D-Quip3NAc). The conformational space sampled by each oligosaccharide was explored using a genetic algorithm implemented in SHAPE.[14]

O-Antigen PS of *E. coli* O5ac: Conformational Search on Oligosaccharide Models. The 20 models of lowest potential energy obtained from the conformational search on each of the initial two hexasaccharide models representing the biological repeating unit of the O-antigen PS of *E. coli* O5ac (each of them built using different conformers of the Ribf residue) were analyzed and clustered according to the ring puckering parameters of the ribofuranose residue and the torsion angles Φ and Ψ across the different glycosidic linkages. The conformation of the ribofuranose ring was analyzed in the 40 models using the method described by Cremer and Pople,[26] and the conformers clustered in two different groups. The major population comprised conformations that existed in the

northern hemisphere[27] of the pseudorotational wheel (with a region of conformational space between E_2 and ^3E), whereas the minor population comprised conformers present in the southern hemisphere (conformations ranging from ^2E to $^4T_3$). The results of this clustering are summarized in Figure 2a. Analysis of the torsion angles Φ and Ψ across the different glycosidic linkages revealed several conformational families (Figure 2b). These results are compiled in Table 1, which shows that in most of the cases the major conformational state

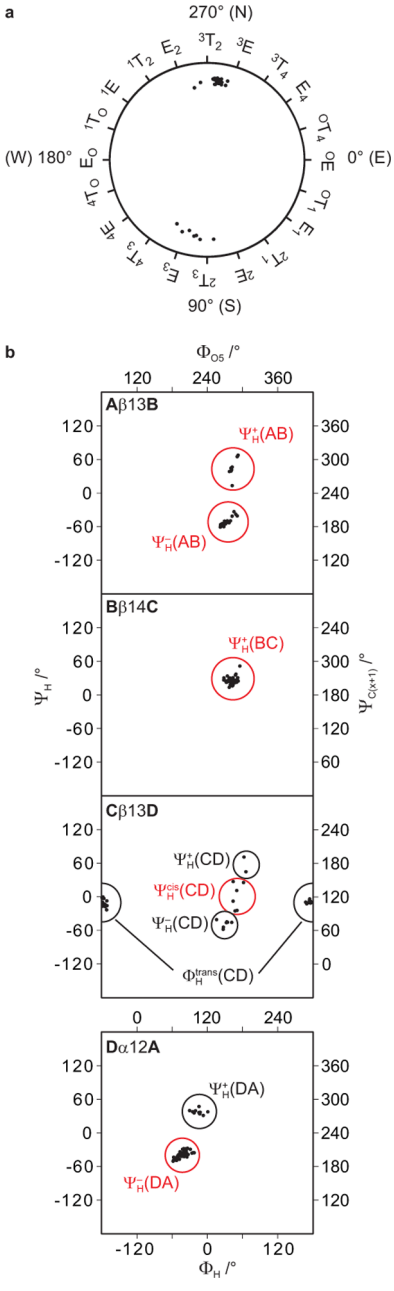

Figure 2. (a) Conformation of the ribofuranose ring (residue **B**) as a function of the puckering parameters Q and φ,[26,45] where the radius of the pseudorotation wheel is Q = 0.5 Å. (b) Scatter plots of Ψ vs Φ obtained from the conformational sampling on the two hexasaccharide models representing the biological repeating unit of the O-antigenic PS of *E. coli* O5ac. The different conformational families found across each glycosidic linkage (indicated in the upper left corner of each plots) are annotated, and those that are consistent with the experimental data are highlighted in red.

is the one for which the *exo*-anomeric effect prevails ($\Phi_H \sim 40°$ for β-D-sugars and $\Phi_H \sim -40°$ for α-D-sugars), with the exception of the β-D-Galp-(1→3)-α-D-Gal*p*NAc linkage (**C**β**13D**) where the Φ_H^{trans} conformational state ($\Phi_H \sim 180°$) was also represented. In all the models in which the *exo*-anomeric conformational state is present, the Ψ_H glycosidic torsion angles lead to *cis*- and *gauche*-conformations, where the anomeric proton and the proton on the glycosyloxylated carbon are in close spatial proximity. At the β-D-Qui*p*3NAc-(1→3)-β-D-Rib*f* and α-D-Gal*p*NAc-(1→2)-β-D-Qui*p*3NAc linkages (**A**β**13B** and **D**α**12A**, respectively), both the Ψ_H^+ and Ψ_H^- states (defined by having the torsion angle $\Psi_H > 0°$ and $< 0°$, respectively) are populated. In the former, the Ψ_H^- state is associated with the Rib*f* (residue **B**) in $^3T_2$-^3E (North) conformations, whereas the Ψ_H^+ state is mainly associated with ^2E-$^4T_3$ conformations (South) of the ribofuranoside ring. At the β-D-Rib*f*-(1→4)-β-D-Gal*p* linkage (**B**β**14C**) only the Ψ_H^+ state is present, whereas at the β-D-Gal*p*-(1→3)-α-D-Gal*p*NAc linkage (**C**β**13D**) three different states could be identified for those conformations in which the *exo*-anomeric effect prevails: *gauche*+ ($90° > \Psi_H^+ > 30°$), *cis* ($30° > \Psi_H^{cis} > -30°$), and *gauche*− ($-30° > \Psi_H^- > -90°$).

Relevant proton−proton distances (r_{ij}) were extracted from the models and plotted as a function of the dihedral angles Ψ_H in the respective glycosidic linkages. Each of the different conformational families identified in Table 1 give rise to a very distinctive set of effective proton−proton distances (Figure 3), which allows for comparison with experimental observations.

O-Antigen PS of *E. coli* O5ac: NMR Spectroscopy. The average number of repeating units of the O-antigen PS of *E. coli* O5ac was determined by integration of the resonances at δ 4.78 (H1 in **A**) and 4.60 (H1 in **A′**) in the ^1H NMR spectrum, and corresponded to ∼14 repeating units. The conformations of the O-antigen PS from *E. coli* O5ac were examined using proton−proton distances obtained from ^1H,^1H-NOESY experiments. The ^1H chemical shifts assignments have been reported earlier.[7] The ^1H,^1H-NOESY spectrum of the O-antigen PS from *E. coli* O5ac shows a number of strong intraresidue correlations as well as inter-residue correlations across the glycosidic linkages (Figure 4a). The cross-peak volumes measured at different mixing times were used to generate NOE build-up curves,[28] which were analyzed using the PANIC (Peak Amplitude Normalization for Improved Cross-Relaxation) approach.[29] Proton−proton cross-relaxation rates were extracted from the slope of these curves (Figure 4b) and the calculated intraresidue distance between H1 and H2 of the Gal*p*NAc residue (**D**) was used as reference to obtain the unknown distances using the isolated spin-pair approximation (ISPA).[30] Cross-relaxation rates obtained for the different proton pairs and their corresponding effective distances are compiled in Table 2 and compared to those obtained by conformational sampling.

At the β-D-Qui*p*3NAc-(1→3)-β-D-Rib*f* linkage (**A**β**13B**), three distances were determined from the anomeric proton of residue **A** to H2, H3, and H4 of residue **B** (3.08, 2.42, and 2.87 Å, respectively). These distances were compared with the calculated distances obtained for each of the two populations identified by molecular modeling (Ψ_H^-(AB) and Ψ_H^+(AB) in Figure 3a−c). The experimental data can only be explained by considering a population distribution of approximately 75 and 25% of the conformational families Ψ_H^-(AB) and Ψ_H^+(AB), respectively. The calculated values for the averaged populations (2.95, 2.37, and 2.86 Å, respectively) then differ only by 0.13,

dx.doi.org/10.1021/bm400354y | *Biomacromolecules* 2013, 14, 2215−2224

Table 1. Averaged Torsion Angles for Each of the Conformational Families Identified in the Conformational Sampling of the Two Hexasaccharides Representing the Biological Repeating Unit of the O-Antigen PS from *E. coli* O5ac[a]

		avg values (°)			avg values (°)		
glycosidic linkage	family	Φ_{O5}	Φ_H	state	$\Psi_{C(x+1)}$	Ψ_H	state
AB	Ψ_H^-(AB)[b]	271 [262,290]	31 [22,51]	*exo*	185 [177,203]	−53 [−61, −33]	*gauche*−
	Ψ_H^+(AB)[c]	283 [278,291]	43 [38,52]		278 [248,300]	45 [13,68]	*gauche*+
BC	Ψ_H^+(BC)	279 [266,291]	42 [28,56]	*exo*	144 [134,170]	25 [14,52]	*gauche*+
CD	Ψ_H^-(CD)	269 [255,280]	30 [16,42]	*exo*	73 [63,80]	−48 [−58, −41]	*gauche*−
	Ψ_H^{cis}(CD)	288 [282,301]	50 [44,62]	*exo*	120 [96,145]	1 [−25,27]	*cis*
	Ψ_H^+(CD)	302 [300,304]	64 [63,66]	*exo*	174 [161,187]	58 [45,71]	*gauche*+
	Φ_H^{trans}(CD)	63 [50,72]	180 [168,189]	*trans*	111 [99,120]	−10 [−23,0]	
DA	Ψ_H^-(DA)	78 [62,96]	−41 [−58, −22]	*exo*	203 [192,213]	−38 [−51, −28]	*gauche*−
	Ψ_H^+(DA)	104 [90,120]	−15 [−30,1]	*exo*	273 [268,283]	37 [31,47]	*gauche*+

[a]The maximum and minimum torsion angle values considered for each conformational family are indicated in square brackets. [b]Associated with the ribofuranose ring in $^3T_2$−^{3}E (N) conformations. [c]Associated with the ribofuranose ring in E$_2$−$^3T_2$ (N) or ^{2}E−$^4T_3$ (S) conformations.

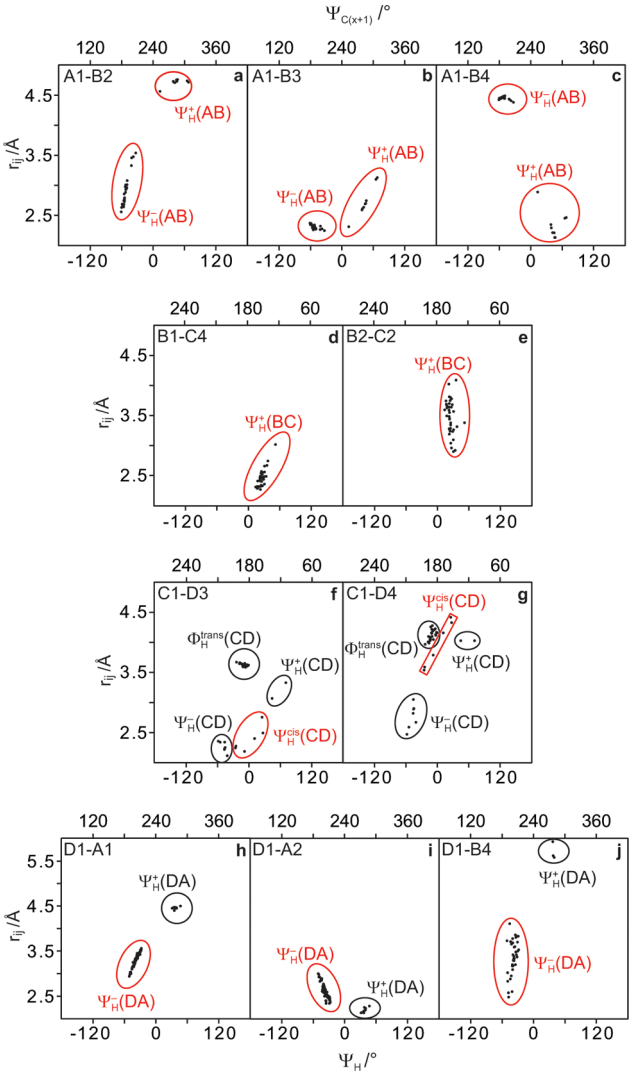

Figure 3. Scatter plots of r_{ij} vs Ψ obtained from conformational sampling of the two hexasaccharide models representing the biological repeating unit of the O-antigenic PS of *E. coli* O5ac. The proton pairs considered in the ordinate axis are annotated in the upper left corner of each plot. Ellipses and rectangles were used to highlight the data from the different conformational families, which were clustered based on the sign and magnitude of the Ψ and Φ torsion angles. The families that explain the experimental data are shown in red.

0.05, and 0.01 Å, respectively, from the experimental values. At the *β*-D-Rib*f*-(1→4)-*β*-D-Gal*p* linkage (**B***β*14**C**), two distances were determined: the shorter one being 2.52 Å (between H1 of residue **B** and H4 of residue **C**) and the longer one being 3.34 Å (between H2 of residue **B** and H2 of residue **C**). These results are comparable to the distances calculated from the low-energy models obtained from the conformational sampling (2.43 and 3.40 Å, respectively), which only comprise conformers of a Ψ_H^+(BC) family (Figure 3d,e). At the *β*-D-Gal*p*-(1→3)-*α*-D-Gal*p*NAc linkage (**C***β*13**D**), the determination of the cross-relaxation rate between H1 of residue **C** and H3 of residue **D** was hampered by the overlapping of the corresponding cross-peak with two peaks arising from intra-residue correlations in residue **C** (H1−H3 and H1−H5). Therefore, the inter-residue distance was deduced from the cross-relaxation rate obtained for the three overlapping cross-peaks (1.525 and 1.396 s^{-1} at a ^{1}H frequency of 700 and 500 MHz, respectively) by subtracting the theoretical cross-relaxation rates predicted[31,32] for each of the intraresidue cross-peaks ($r_{H1,H3}$ = 2.61 Å and $r_{H1,H5}$ = 2.41 Å). Using this approach, we found that the distance between H1 of residue **C** and H3 of residue **D** is actually very short (∼2.21 Å), which is an important conformational restriction when examining the different conformational states found across this glycosidic linkage. In addition, no cross-peak of significant intensity was observed between H1 of residue **C** and H4 of residue **B**, indicating that these two atoms are separated by a distance longer than 3.5 Å (taking as reference the longest distance determined in this study, i.e., between the anomeric protons of residues **A** and **D**). This data can be explained by the proton−proton distances measured in the conformers of the Ψ_{CD}^{cis} family (2.35 and 3.87 Å, respectively) and indicate that the remaining subfamilies (Ψ_H^-(CD), Ψ_H^+(CD), and Φ_H^{trans}(CD) in Figure 3f,g) are not significantly populated. Furthermore, the ^{13}C NMR chemical shifts for the carbon atoms at this glycosidic linkage, that is, C1 in residue **C** and C3 in residue **D**, are highly similar to those in *β*-D-Gal*p*-(1→3)-*α*-D-Gal*p*NAc-OMe,[33] indicating that the conformational preferences in the polysaccharide are similar to those of the constituent disaccharide. At the *α*-D-Gal*p*NAc-(1→2)-*β*-D-Qui*p*3NAc linkage (**D***α*12**A**) two *trans*-glycosidic effective distances could be determined, a short one between H1 in residue **D** and H2 in residue **A** (2.69 Å), and a long one between H1 of residue **D** and H1 of residue **A** (3.50 Å, determined only at the higher field). These results are consistent with the averaged proton−proton distances calculated in the conformers of the Ψ_H^-(DA) family (2.58 and

dx.doi.org/10.1021/bm400354y | *Biomacromolecules* 2013, 14, 2215−2224

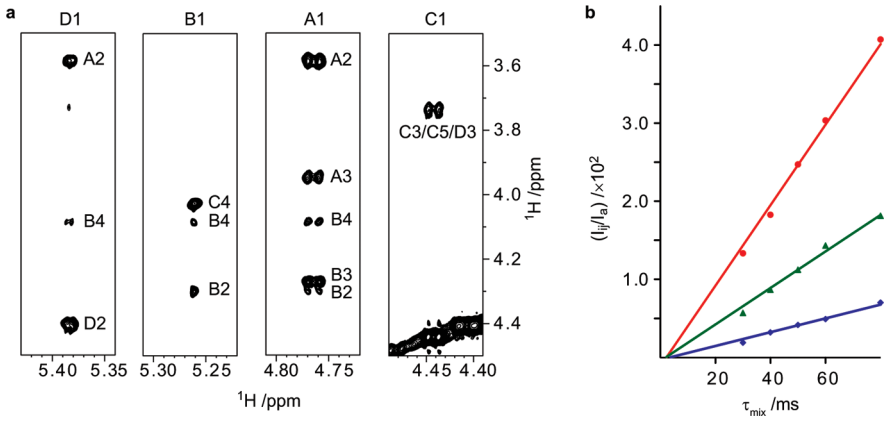

Figure 4. (a) Selected regions of the 2D ^{1}H,^{1}H-NOESY spectrum of the O-antigen PS of *E. coli* O5ac recorded at a ^{1}H frequency of 700 MHz and with a mixing time (τ_{mix}) of 80 ms. Correlations from the anomeric protons are annotated. (b) Plots of the normalized volume intensities vs mixing time for the intraresidue correlation between H1 and H2 of Gal*p*NAc (red filled circle), the *trans*-glycosidic correlation between H1 of Gal*p*NAc and H2 of Qui*p*3NAc (green filled triangle) and the long-range correlation between H1 of Gal*p*NAc and H4 of Rib*f* (blue filled diamond). The data were obtained from 2D ^{1}H,^{1}H-NOESY experiments recorded at a ^{1}H frequency of 700 MHz.

Table 2. Cross-Relaxation Rates and Effective Distances Determined for the O-Antigen PS from *E. coli* O5ac from 2D ^{1}H,^{1}H-NOESY Experiments at a ^{1}H Frequency of 500 and 700 MHz[a]

^{1}H−^{1}H correlation	σ_{ij} 700 MHz (×10^3 s^{-1})	σ_{ij} 500 MHz (×10^3 s^{-1})	r_{ij} (Å)	r_{calc} (Å)	averaged populations[b] r_{calc} (Å)
A1-B2	103	n.d.	3.08	**2.82** (Ψ_H^-(AB))/**4.71** (Ψ_H^+(AB))	2.95 [3:1]
A1-B3	446	406	2.42	**2.31** (Ψ_H^-(AB))/**2.65** (Ψ_H^+(AB))	2.37 [3:1]
A1-B4	159	144	2.87	**4.45** (Ψ_H^-(AB))/**2.29** (Ψ_H^+(AB))	2.86 [3:1]
B1-C4	354	311	2.52	**2.43** (Ψ_H^+(BC))	
B2-C2	64	n.d.	3.34	**3.40** (Ψ_H^+(BC))	
C1-D3[c]	788[c]	690[c]	2.21	2.25 (Ψ_H^-(CD))/**2.35** (Ψ_H^{cis}(CD))/3.18 (Ψ_H^+(CD))/3.63 (Φ_H^{trans}(CD))	
C1-D4	n.o.	n.o.	>3.50	2.72 (Ψ_H^-((CD))/**3.87** (Ψ_H^{cis}(CD))/4.60 (Ψ_H^+(CD))/4.12 (Φ_H^{trans}(CD))	
D1-A1	49	n.o.	3.50	**3.28** (Ψ_H^-(DA))/4.46 (Ψ_H^+(DA))	
D1-A2	234	213	2.69	**2.58** (Ψ_H^-(DA))/2.18 (Ψ_H^+(DA))	
D1-B4	74	64	3.28	**3.19** (Ψ_H^-(DA))/5.70 (Ψ_H^+(DA))	
D1-D2[d]	463	427	2.40[d]	**2.40**	
D4-D5	446	395	2.42	**2.47**	
A1-A3	279	258	2.61	**2.59**	

[a]Calculated distances are given for the different conformational families identified; those values that are consistent with the experimental data are highlighted in bold. [b]Population ratio of families indicated in brackets. [c]Overlapping with C1/C3 and C1/C5. The cross-relaxation rate was deduced by subtracting the theoretical values calculated for the intraresidue correlations. [d]Distance used as reference. n.d. = not determined due to spectral overlap. n.o. = not observed or at the noise level.

3.28 Å, respectively) (Figure 3h,i). In addition, a long distance correlation was observed between H1 in residue **D** and H4 in residue **B** (3.28 Å), which differs by <0.1 Å of the average value obtained for conformers of the Ψ_H^-(DA) family ($r_{D1,B4}$ = 3.19 Å; Figure 3j), providing additional evidence that the Ψ_H^+(DA) conformational family does not represent a significant contribution to the experimental observations ($r_{D1,B4}$ = 5.70 Å).

O-Antigen PS of *E. coli* O5ab: Conformational Search on Oligosaccharide Models. In the 2D ^{1}H,^{1}H-NOESY spectrum of the O-antigen PS from *E. coli* O5ab a number of intra- and inter-residue correlations similar to those observed in the ^{1}H,^{1}H-NOESY spectrum of the O-antigen PS from *E. coli* O5ac were identified across the glycosidic linkages **A**β13**B**, **B**β14**C**, and **C**β13**D**. This observation indicates that the conformations across these linkages are similar to those observed for the O-antigen PS from *E. coli* O5ab. Based on this observation, we focused the analysis of the O-antigen PS from *E. coli* O5ab mainly from the point of view of the α-D-Gal*p*NAc-(1→4)-β-D-Qui*p*3NAc linkage (**D**α14**A**), which is the only structural difference with respect to the O-antigen PS from *E. coli* O5ac.

The 20 models of lowest potential energy obtained from the conformational search on each of the two hexasaccharides representing the biological repeating unit of the O-antigen PS from *E. coli* O5ab (each of them built from a different Rib*f* conformer) were analyzed and clustered according to the conformational states across the α-D-Gal*p*NAc-(1→4)-β-D-Qui*p*3NAc glycosidic linkage. Three conformational families were identified, all corresponding to conformational states where the *exo*-anomeric effect is predominant (Figure 5a and Table 3). The two major families correspond to conformers where the torsion angle Ψ_H leads to *gauche*-conformations, and both Ψ_H^+ and Ψ_H^- states are represented. In addition, a Φ_H^{trans} conformational state was observed in a few models (where the anomeric carbon of residue **D** and H4 of residue **A** are in an antiperiplanar arrangement). The distances from H1 of the Gal*p*NAc residue (**D**) to relevant protons in the Qui*p*3NAc

dx.doi.org/10.1021/bm400354y | *Biomacromolecules* 2013, 14, 2215−2224

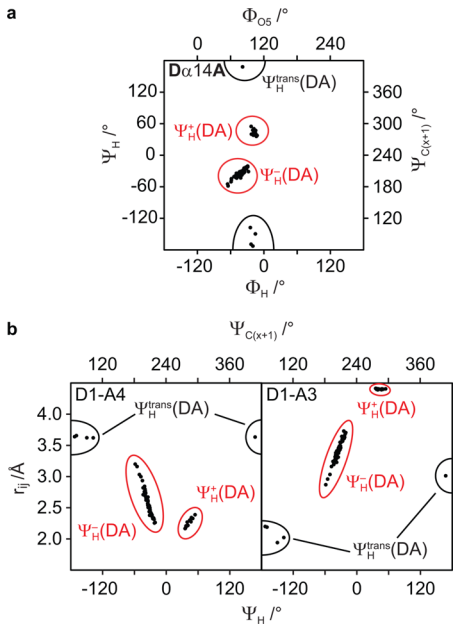

Figure 5. Scatter plots of (a) Ψ(DA) vs Φ(DA) and (b) r_{ij} vs Ψ(DA) obtained from the hexasaccharide models representing the biological repeating unit of the O-antigenic PS of *E. coli* O5ab. In the latter, the proton pairs considered in the ordinate axis are annotated in the upper left corner of each plot. Ellipses were used to highlight the data from the different conformational families, which were clustered based on the sign and magnitude of the Ψ and Φ torsion angles. The conformational families that explain the experimental data are shown in red.

residue (**A**) were extracted from the models and plotted as a function of the dihedral angle Ψ(DA) (Figure 5b).

O-Antigen PS of *E. coli* O5ab: NMR Spectroscopy. The number of repeating units of the O-antigen PS of *E. coli* O5ab was determined by integration of the resonances at δ 4.62 and 4.60 (H1 in **A** and H1 in **A′**) and 1.32 (H6 in **A′**) in the ^{1}H NMR spectrum (Figure 6a), and corresponded to ∼10 repeating units. In order to measure effective proton−proton distances, selective excitation of the anomeric proton of the Gal*p*NAc residue (**D**) was carried out using one-dimensional ^{1}H,^{1}H-NOESY experiments (Figure 6b) to generate NOE build-up curves (Figure 6c) that were analyzed in detail using the same approach as described above. Proton−proton cross-relaxation rates were extracted from the slope of the NOE build-up curves, and a reference distance of 2.39 Å between H1 and H2 of the Gal*p*NAc residue (**D**) was used for distance calibration. These results are compiled in Table 4. The effective distance between H1 of the Gal*p*NAc (residue **D**) and H4 of the Qui*p*3NAc residue (**A**) determined experimentally corresponded to 2.39 Å. This value is slightly shorter than the average distance measured in conformers of the Ψ_H^+(DA) family (2.56 Å) but slightly longer than the average distance obtained from models of the Ψ_H^-(DA) conformational family (2.24 Å). Therefore, both models considered independently or as a mixed contribution, may explain the experimental data. The effective distance between H1 of the Gal*p*NAc residue (**D**) and H3 of the Qui*p*3NAc residue (**A**) determined experimentally (3.20 Å) is slightly longer than the average distance obtained from models of the Ψ_H^-(DA) conformational family (2.91 Å) and significantly much shorter than the average distance obtained from models of the Ψ_H^+(DA) (4.40 Å) conformational family. If a contribution of both conformational families is considered, with a population distribution of about 50% for each of them, then excellent agreement is observed between experimental and calculated values (Table 4). The Φ_H^{trans}(DA) conformational family does not represent a significant contribution to the distance determined experimentally, as the average values calculated from these models differ considerably from the experimental data.

Molecular Modeling of the O-Antigen PS of *E. coli* O5ac and O5ab. Several 3D models of the O-antigen PSs of *E. coli* O5ac and O5ab were built using the CarbBuilder software.[34] The torsion angles at the different glycosidic linkages used to build the models, as well as the conformation associated to the ribofuranoside residue, are compiled in Table 5. Two models were constructed for the O-antigen PS of *E. coli* O5ac, which differ from each other in the conformation of the ribofuranose residue and the torsion angles around the glycosidic linkage **A**β**13B** (Φ(AB) and Ψ(AB)) (Figure 7a,b). Four different models were needed to explain the conformational behaviors of the O-antigen PS of *E. coli* O5ab, in which the same parameters as above were considered, in conjunction with two possible conformational families around the glycosidic linkage **D**α**14A**, arising from differences in the torsion angles Φ(DA) and Ψ(DA) (Figure 7c−f). Thus, the left-hand side models of Figure 7a,c,e represent conformers in which the Rib*f* ring adopts a north conformation, whereas the right-hand side models represent those conformers in which a south conformation of the ribofuranose ring is preferred.

Structural Similarities and Cross-Reactivity within *E. coli* Serogroups. A minor spin system, corresponding to a terminal β-D-Qui*p*3NAc residue, was identified in both PSs and attributed to the monosaccharide residue located at the terminal nonreducing end of the polysaccharide. As anticipated, this is in agreement with the biosynthesis taking place by the Wzx/Wzy-dependent pathway,[9] in which a GalNAc residue initiates the biosynthesis of the oligosaccharide building block, and therefore, this monosaccharide residue is expected to be located at the reducing end of the biological repeating unit. Consequently, the O-antigen gene cluster of these two polysaccharides is expected to be almost identical, differing only in the gene that encodes the Wzy polymerase.

Given the flexibility of these polysaccharides, inferred by the number of different conformations they can adopt in solution, potentially antigenic common motifs for antibodies that bind to

Table 3. Averaged Torsion Angles from the Conformational Sampling of the Two Hexasaccharides Representing the Biological Repeating Unit of the O-Antigen PS from *E. coli* O5ab

		avg values (°)			avg values (°)		
glycosidic linkage	family	Φ_{O5}	Φ_H	state	$\Psi_{C(x+1)}$	Ψ_H	state
DA	Ψ_H^-(DA)	77 [55,91]	−43[−65, −28]	*exo*	206 [185,220]	−35 [−58, −21]	*gauche−*
	Ψ_H^+(DA)	103 [97,107]	−17 [−23, −12]	*exo*	279 [272,291]	42 [36,55]	*gauche+*
	Ψ_H^{trans}(DA)	96 [82,104]	−24 [−38, −15]	*exo*	80 [50,107]	−164 [−192, −138]	*trans*

dx.doi.org/10.1021/bm400354y | *Biomacromolecules* 2013, 14, 2215−2224

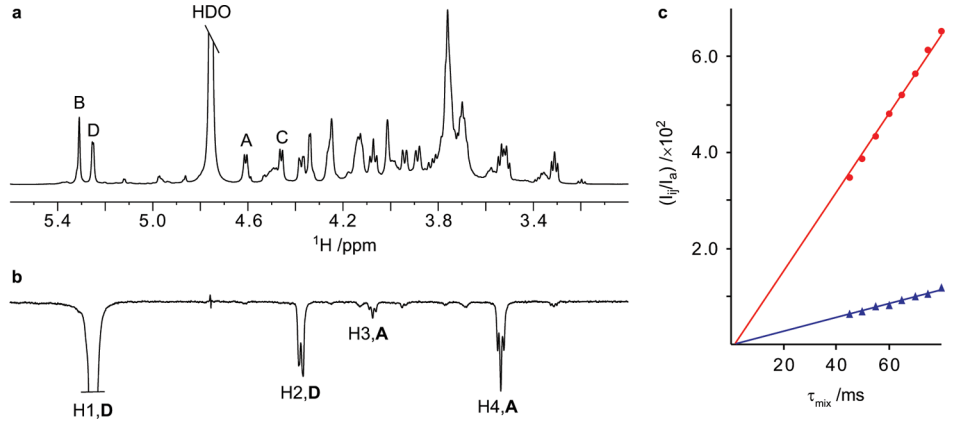

Figure 6. Comparison of (a) the ^{1}H NMR spectrum of the O-antigen PS of *E. coli* O5ab and (b) the 1D ^{1}H,^{1}H-SPFGSE NOESY spectrum (τ_{mix} 80 ms) with selective excitation of the H1 resonance of Gal*p*NAc (residue **D**). (c) Plots of the normalized intensities vs mixing time obtained for the *trans*-glycosidic correlations between H1 of Gal*p*NAc (residue **D**) and H3 (blue filled triangle) and H4 (red filled circle) of Qui*p*3NAc (residue **A**).

Table 4. Cross-Relaxation Rates and Effective Distances Determined for the O-Antigen PS from *E. coli* O5ab from 1D ^{1}H,^{1}H-NOESY Experiments at a ^{1}H Frequency of 700 MHz[a]

^{1}H–^{1}H correlation	σ_{ij} (×10^3 s^{-1})	r_{ij} (Å)	r_{calc} (Å)	averaged populations[b]
D1-A3	144	3.20	**2.91** (Ψ_H^-(DA))/**4.40** (Ψ_H^+(DA))/2.14 (Ψ_H^{trans}(DA))	3.22 [1:1]
D1-A4	819	2.39	**2.56** (Ψ_H^-(DA))/**2.24** (Ψ_H^+(DA))/3.36 (Ψ_H^{trans}(DA))	2.36 [1:1]
D1-D2[c]	824	2.39[c]	2.39	

[a]Calculated distances are given for the different conformational families identified; those values that are consistent with the experimental data are highlighted in bold. [b]Population ratio of families indicated in brackets. [c]Distance used as reference.

internal epitopes are difficult to recognize, when focusing exclusively on the antigen structure. Moreover, one also has to consider that the PS can undergo a protein-induced conformational change when bound to the monoclonal antibodies, and then the conformation in the bound state may differ from the preferred conformations found in solution.[35,36] Herein, we have shown that these polysaccharides can adopt different conformations in solution, and this may have implications in the cross-reactivity observed between the *E. coli* O5ac and O5ab serogroups. For instance, out of several conformational states available in solution, one of them may represent a conformation similar to that needed in the bound state with a specific monoclonal antibody, or on the other hand, the antibody–antigen interaction may benefit from the possibility that the antigen accommodates itself into the specific binding pocket upon interaction with the monoclonal antibody. The structures illustrated in Figure 7 represent canonical models where different portions of the PS may adopt different conformations, leading to a very large number of possible 3D structures and, consequently, an alternative approach has to be considered in order to specifically identify common internal epitopes in these two PS (i.e., studies of the dynamic interactions of monoclonal antibodies with both polysaccharides).

On the other hand, terminal epitopes are also likely to be recognized by the protective antibodies targeting the infection,[6,37,38] and in the case of *Vibrio cholera* O1, they have proven to play a dominant role in the immunological differentiation or cross-reactivity between different serotypes.[39,40] The cross-reactivity observed between strains of the O5, O65, O70, and O71 serogroups[4] may be explained in terms of antibodies recognizing terminal epitopes. All the O-antigens that belong to these serogroups contain a D-Qui*p*3NAc residue in their repeating units,[41−43] which can be anticipated to be located at the nonreducing end of the biological repeating unit[9] and, thus, at the terminal nonreducing end of the PSs. Antibodies binding to terminal epitopes have been proposed to have a "cavity-like" binding site that can accommodate a maximum of five sugar residues, and thus, they are expected to have more affinity and avidity than antibodies targeting internal epitopes (which are proposed to have a "groove-type" binding site and therefore lower expected complementarity).[5,6] The very strong cross-reactivity observed between strains of the

Table 5. Torsion Angles and Conformation of the Ribofuranose Residue Used As Input Information in the CarbBuilder software[34] To Generate the Different Molecular Models of the O-Antigen PSs of *E. coli* O5ac and O5ab Shown in Figure 7

		torsion angle (°)								
		AB		BC		CD		DA		
PS	entry	Φ_H	Ψ_H	Φ_H	Ψ_H	Φ_H	Ψ_H	Φ_H	Ψ_H	Rib*f* conformation
O5ac	1	31	−53	42	25	50	1	−41	−38	$^3T_2$-^3E (N)
	2	43	45	42	25	50	1	−41	−38	$^2T_3$-E_3 (S)
O5ab	3	31	−53	42	25	50	1	−43	−35	$^3T_2$-^3E (N)
	4	43	45	42	25	50	1	−43	−35	$^2T_3$-E_3 (S)
	5	31	−53	42	25	50	1	−17	42	$^3T_2$-^3E (N)
	6	43	45	42	25	50	1	−17	42	$^2T_3$-E_3 (S)

dx.doi.org/10.1021/bm400354y | *Biomacromolecules* 2013, 14, 2215−2224

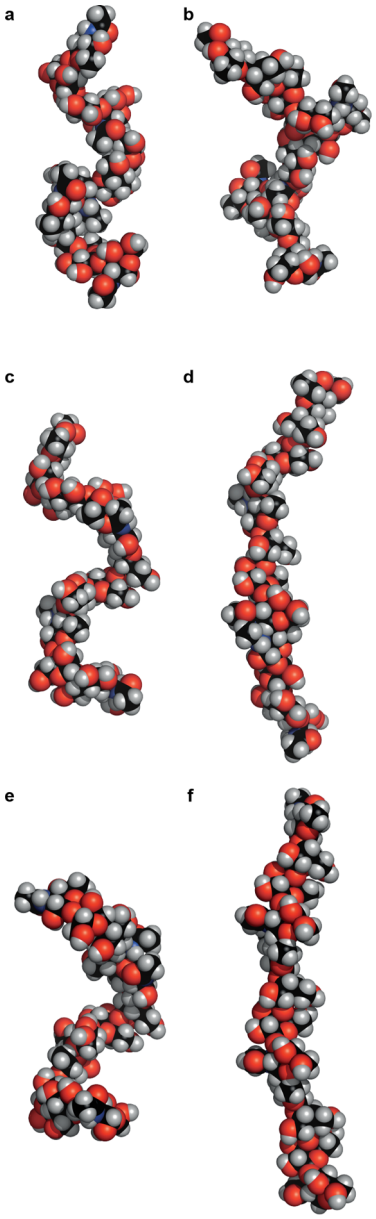

Figure 7. Space filling representation of the two conformations of the O-antigen PS of *E. coli* O5ac built using the information of entries 1 and 2 of Table 5 (panels a and b, respectively) and the four conformations of the O-antigen PS of *E. coli* O5ab built using the information of entries 3–6 of Table 5 (panels c, d, e, and f, respectively). All the models shown in this picture were constructed using three biological repeating units and the CarbBuilder software.[34].

O5ac and O5ab subgroups of *E. coli* can also be perceived in terms of a higher epitope-binding site complementarity. In these two subgroups, not only the monosaccharide but the tetrasaccharide moiety located at the terminal nonreducing end of both polysaccharides share exactly the same structure and conformational behaviors and, thus, will be indistinguishable from the point of view of the protective antibodies targeting this region of the PS. On the other hand, *E. coli* O114 has been reported to present cross-reactivity only with *E. coli* O5, but not with the O65, O70, or O71 serogroups. It is interesting to note that the only difference in the trisaccharide moiety located at the terminal nonreducing end of the O-antigen PS of *E. coli* O114, with respect to that of the O5ac and O5ab serogroups, is the *N*-substituent of the β-D-Qui*p*3N residue (*N*-acetyl-L-seryl instead of *N*-acetyl).[44] Thus, a modification in the Qui*p*3N residue seems to be critical in the cross-reactivity pattern observed between these serogroups, showing a possible critical implication of antibodies that bind to terminal epitopes (i.e., the antibodies that recognize terminal epitopes, induced by strains of the O5, O65, O70 and O71 serogroups, may not be capable to recognize the Qui*p*3NAcyl residue located at the terminal nonreducing end of the O-antigen PS of *E. coli* O114, and vise versa). The cross-reactivity between *E. coli* O5 and O114 (which contains an *N*-acetyl-D-glucosamine residue at the reducing end of the biological repeating unit instead of a *N*-acetyl-D-galactosamine residue), can then be explained in terms of recognition of internal epitopes, which is expected due the high structural similarity shared by the repeating units of the O-specific polysaccharides belonging to these two serogroups.

CONCLUSIONS

In this study we explored the conformational preferences of the O-antigen PSs of *E. coli* O5ac and O5ab. Intra- and inter-residue distances were obtained from ^{1}H,^{1}H-NOESY experiments and were used to evaluate the different conformational families identified from the molecular models of the repeating units of each O-antigen polysaccharide. The torsion angles as well as the conformations of the ribofuranose residue that explained the experimental distances were employed to generate the corresponding polysaccharide models. According to our results, there is not a single unique 3D macrostructure that can explain the conformational behavior of these two polysaccharides; however, an agreement between experimentally measured and calculated distances could be obtained by considering an averaging of several low energy conformations. Two different models were built to represent the preferred conformations of substantial portions of the O-antigen PS exposed on the surface of *E. coli* O5ac, whereas four different models were needed for the O-antigen PS of *E. coli* O5ab. The possibility of these PSs to adopt different conformations may have an implication in the cross-reactivity observed between strains of the *E. coli* O5ac and O5ab serogroups, because they could easily adapt their conformations to match the antibodies binding site requirements. In addition, the identification of the biological repeating unit of the polysaccharides showed that the terminal epitopes of these O-antigens are identical and, consequently, indiscernible from the point of view of specific antibodies targeting this part of the polysaccharide.

ASSOCIATED CONTENT

Supporting Information

The PDB files of the 3D models of the O-antigen PSs of *E. coli* O5ac and O5ab shown in Figure 7. This material is available free of charge via the Internet at http://pubs.acs.org.

AUTHOR INFORMATION

Corresponding Author

*E-mail: serge.perez@cermav.cnrs.fr; gw@organ.su.se.

Author Contributions

‡These authors contributed equally to this work.

Notes

The authors declare no competing financial interest.

■ ACKNOWLEDGMENTS

This work was supported by grants from the Swedish Research Council and The Knut and Alice Wallenberg Foundation. The research leading to these results has received funding from the European Commission's Seventh Framework Programme FP7/2007-2013 under Grant Agreement No. 215536.

■ REFERENCES

(1) Kaper, J. B.; Nataro, J. P.; Mobley, H. L. *Nat. Rev. Microbiol.* **2004**, *2*, 123−140.
(2) Knirel, Y. A. In *Bacterial Lipopolysaccharides. Structure, Chemical Synthesis, Biogenesis and Interaction with Host Cells*; Knirel, Y. A., Valvano, M. A., Eds.; Springer: Vienna, 2011; pp 41−115.
(3) Weintraub, A. *Carbohydr. Res.* **2003**, *338*, 2539−2547.
(4) Ørskov, F.; Ørskov, I. *Meth. Microbiol.* **1984**, *14*, 43−112.
(5) Cisar, J.; Kabat, E. A.; Dorner, M. M.; Liao, J. *J. Exp. Med.* **1975**, *142*, 435−459.
(6) Roche, M. I.; Lu, Z.; Hui, J. H.; Sharon, J. *Hybridoma* **2011**, *30*, 19−28.
(7) Urbina, F.; Nordmark, E.-L.; Yang, Z.; Weintraub, A.; Scheutz, F.; Widmalm, G. *Carbohydr. Res.* **2005**, *340*, 645−650.
(8) MacLean, L. L.; Perry, M. B. *Biochem. Cell Biol.* **1997**, *75*, 199−205.
(9) Stenutz, R.; Weintraub, A.; Widmalm, G. *FEMS Microbiol. Rev.* **2006**, *30*, 382−403.
(10) Berman, H. M.; Westbrook, J.; Feng, Z.; Gilliland, G.; Bhat, T. N.; Weissig, H.; Shindyalov, I. N.; Bourne, P. E. *Nucleic Acids Res.* **2000**, *28*, 235−242.
(11) Pérez, S.; Gautier, C.; Imberty, A. In *Carbohydrates in Chemistry and Biology*; Ernst, B., Hart, G. W., Sinay, P., Eds.; Wiley-VCH: Verlag GmbH: Weinheim, Germany, 2008; Vol. *32*, pp 969−1001.
(12) Clark, M.; Cramer, R. D., III; Van Opdenbosch, N. *J. Comput. Chem.* **1989**, *10*, 982−1012.
(13) Imberty, A.; Bettler, E.; Karababa, M.; Mazeau, K.; Petrová, P.; Pérez, S. In *Perspectives in Structural Biology*; Vijayan, M., Yathindra, N., Kolaskar, A. S., Eds.; Universities Press (India) Limited: Hyderabad, 1999; pp 392−409.
(14) Rosen, J.; Miguet, L.; Pérez, S. *J. Cheminform.* **2009**, *1*, 16.
(15) Allinger, N. L.; Li, F.; Yan, L.; Tai, J. C. *J. Comput. Chem.* **1990**, *11*, 868−895.
(16) Allinger, N. L.; Yuh, Y. H.; Lii, J.-H. *J. Am. Chem. Soc.* **1989**, *111*, 8551−8566.
(17) Pérez, S.; Imberty, A.; Engelsen, S. B.; Gruza, J.; Mazeau, K.; Jimenez-Barbero, J.; Poveda, A.; Espinosa, J.-F.; van Eyck, B. P.; Johnson, G.; French, A. D.; Kouwijzer, M. L. C. E.; Grootenuis, P. D.; Bernardi, A.; Raimondi, L.; Senderowitz, H.; Durier, V.; Vergoten, G.; Rasmussen, K. *Carbohydr. Res.* **1998**, *314*, 141−155.
(18) Thrippleton, M. J.; Keeler, J. *Angew. Chem., Int. Ed.* **2003**, *42*, 3938−3941.
(19) Kupče, Ē. *Meth. Enzymol.* **2002**, 82−111.
(20) Tannús, A.; Garwood, M. *NMR Biomed.* **1997**, *10*, 423−434.
(21) Böhlen, J.-M.; Bodenhausen, G. *J. Magn. Reson., Ser. A* **1993**, *102*, 293−301.
(22) Larsson, E. A.; Staaf, M.; Söderman, P.; Höög, C.; Widmalm, G. *J. Phys. Chem. A* **2004**, *108*, 3932−3937.
(23) Stott, K.; Keeler, J.; Van, Q. N.; Shaka, A. J. *J. Magn. Reson.* **1997**, *125*, 302−324.
(24) Kupče, Ē.; Boyd, J.; Campbell, I. D. *J. Magn. Reson., Ser. B* **1995**, *106*, 300−303.
(25) Wu, D.; Chen, A.; Johnson, C. S. *J. Magn. Reson., Ser. A* **1995**, *115*, 260−264.
(26) Cremer, D.; Pople, J. A. *J. Am. Chem. Soc.* **1975**, *97*, 1354−1358.
(27) Altona, C.; Sundaralingam, M. *J. Am. Chem. Soc.* **1972**, *94*, 8205−8212.
(28) Widmalm, G.; Byrd, R. A.; Egan, W. *Carbohydr. Res.* **1992**, *229*, 195−211.
(29) Macura, S.; Farmer, B. T., II; Brown, L. R. *J. Magn. Reson.* **1986**, *70*, 493−499.
(30) Thomas, P. D.; Basus, V. J.; James, T. L. *Proc. Natl. Acad. Sci. U.S.A.* **1991**, *88*, 1237−1241.
(31) Jonsson, K. H. M.; Pendrill, R.; Widmalm, G. *Magn. Reson. Chem.* **2011**, *49*, 117−124.
(32) Zaccheus, M.; Pendrill, R.; Jackson, T. A.; Wang, A.; Auzanneau, F.-I.; Widmalm, G. *Eur. J. Org. Chem.* **2012**, *2012*, 4705−4715.
(33) Jansson, P.-E.; Widmalm, G. *J. Chem. Soc., Perkin Trans. 2* **1992**, 1085−1090.
(34) Kuttel, M.; Mao, Y.; Widmalm, G.; Lundborg, M. *Proc. 7th IEEE Int. Conf. eScience* **2011**, 395−402.
(35) Bundle, D. R.; Baumann, H.; Brisson, J.-R.; Gagné, S. M.; Zdanov, A.; Cygler, M. *Biochemistry* **1994**, *33*, 5183−5192.
(36) Milton, M. J.; Bundle, D. R. *J. Am. Chem. Soc.* **1998**, *120*, 10547−10548.
(37) Fernandez, C.; Sverremark, E. *Cell. Immunol.* **1994**, *153*, 67−78.
(38) Carlin, N. I.; Bundle, D. R.; Lindberg, A. A. *J. Immunol.* **1987**, *138*, 4419−4427.
(39) Bystrický, S.; Szu, S. C.; Zhang, J.; Kováč, P. *Carbohydr. Res.* **1998**, *314*, 135−139.
(40) Villeneuve, S.; Souchon, H.; Riottot, M.-M.; Mazié, J.-C.; Lei, P.-s.; Glaudemans, C. P. J.; Kováč, P.; Fournier, J.-M.; Alzari, P. M. *Proc. Natl. Acad. Sci. U.S.A.* **2000**, *97*, 8433−8438.
(41) Perry, M. B.; MacLean, L. L. *Carbohydr. Res.* **1999**, *322*, 57−66.
(42) MacLean, L. L.; Perry, M. B. *Carbohydr. Res.* **2010**, *345*, 644−648.
(43) Hu, B.; Perepelov, A. V; Liu, B.; Shevelev, S. D.; Guo, D.; Senchenkova, S. N.; Shashkov, A. S.; Feng, L.; Knirel, Y. A.; Wang, L. *FEMS Immunol. Med. Microbiol.* **2010**, *59*, 161−169.
(44) Dmitriev, B. A.; Lvov, V.; Tochtamysheva, N. V.; Shashkov, A. S.; Kochetkov, N. K.; Jann, B.; Jann, K. *Eur. J. Biochem.* **1983**, *134*, 517−521.
(45) Grůza, J.; Koča, J.; Pérez, S.; Imberty, A. *J. Mol. Struct.: THEOCHEM* **1998**, *424*, 269−280.